Assessment of da Vinci tool and wrist rotations that maximize fluence in photoacoustic-guided surgery: A simulation study

Gareth C. Keene[a] and Muyinatu A Lediju Bell[a,b,c,d]

[a]Johns Hopkins University, Department of Electrical and Computer Engineering, Baltimore, MD
[b]Johns Hopkins University, Department of Computer Science, Baltimore, MD
[c]Johns Hopkins University, Department of Biomedical Engineering, Baltimore, MD
[d]Johns Hopkins University, Department of Oncology, Baltimore, MD

ABSTRACT

In minimally invasive photoacoustic-guided surgical procedures, one approach to achieve required target illumination is to attach light sources to a surgical tool, such as a scissor tool attached to a da Vinci robot for teleoperated surgeries. However, the tool tip can present an obstacle to light transmission when placed in particular orientations. We quantify the optical fluence resulting from different orientations of the da Vinci scissors tool, using Monte Carlo simulations to measure fluence at varying depths below the tissue surface. A metallic model of the da Vinci scissors tool was placed above simulated tissue in an orientation mimicking a surgical procedure. The da Vinci scissors tool was modeled with pivot points corresponding to two joints: (1) the wrist joint, which is near the base of the scissors tool tip and (2) the scissors joint, around which the scissors open and close, closer to the tip of the tool. Light sources representing optical fibers were placed around the base of the tool, facing the tissue. Simulations were performed with 154 total parameter combinations of different positions (i.e., seven wrist joint rotations using a dedicated wrist joint rotation model, seven scissor joint rotations using a dedicated scissor joint rotation model, with each joint in each model additionally rotated about an orthogonal axis, from 0° to -180° in 18° increments). The resulting fluence was measured in a 10 mm radius region of interest (ROI) located 1 mm below the tissue surface under the tool. The maximum normalized fluence difference between two simulated tool orientations was 18-21%. These results establish a new simulation framework to enhance our understanding of the impact of specific tool orientations on the fluence delivered to tissue, which has the potential to impact the associated photoacoustic image quality.

1. INTRODUCTION

Minimally invasive surgeries (e.g., laparoscopy) use slender instruments and *in vivo* lighting to operate within the abdomen through small incisions, significantly reducing patient recovery times and complications.[1] However, laparoscopic procedures can present higher risks when patients have a confluence of conditions.[2] To address some of the most challenging of minimally invasive surgical applications, robotic assistance (e.g., with the da Vinci robot) has gained popularity due to enhanced precision and stereoscopic imaging, which lead to fewer complications, faster recovery, and shorter hospital stays compared to traditional laparoscopy.[3] Despite these advances, visualizing targets concealed by tissue remains a challenge.[2]

Photoacoustic imaging has emerged as a possible technique for minimally invasive surgical procedures, as it enables real-time visualization of tissues.[4] To achieve photoacoustic imaging, a pulsed laser illuminates a target of interest, which absorbs the optical energy and undergoes thermal expansion, followed by contraction and the emission of an acoustic signal. An ultrasound transducer detects the acoustic signal and the location of the image target is determined through signal processing techniques.[4–6]

Combining the advantages of optical and acoustic imaging, photoacoustic imaging has been previously demonstrated to offer potential benefits for surgeries such as neurosurgery,[7–10] liver surgery,[11,12] robot-assisted biopsy guidance,[13] cardiac catheter guidance,[14,15] spinal surgeries,[16–18] and hysterectomies.[19–22] Benefits include functional, high contrast, and depth-specific images of blood vessels, nerves, and other critical structures to target or

Advanced Biomedical and Clinical Diagnostic and Surgical Guidance Systems XXIII, edited by Caroline Boudoux, James W. Tunnell, Proc. of SPIE Vol. 13306, 1330608 · © 2025 SPIE · 1605-7422 · doi: 10.1117/12.3045978

avoid during a surgical procedure. In particular, photoacoustic imaging enables differentiation between different tissue types based on differing levels of optical absorption in the tissue.

When implementing photoacoustic-guided surgeries, one novel approach to illuminate targets is to attach optical fibers directly to surgical tools.[9] This approach offers the potential to differentiate distances between major blood vessels and other critical structures during surgery,[23] without requiring calibrations to determine tool proximity to identified structures. However, in some configurations of tool orientations, tool-attached illumination sources can potentially alter the photoacoustic image.[20] When considering the orientations of tools, it also important to consider the uniformity of the fluence reaching the tissue below as non-uniformity can create difficulty when recovering chromophore distributions.[24]

To overcome the challenges of non-uniform fluence in light profiles and potential tool orientations that degrade photoacoustic image quality, we perform quantitative assessments of light profile changes caused by varying tool orientations. These assessments can support the development of best practices for surgeons operating with photoacoustic image guidance as well as new designs for tool-attached optical illumination systems.

To determine optimal tool orientations with respect to a scissor tool, simulations were performed to quantify fluence within a target area under multiple fiber-attached tool orientations. The simulation environment included air, tissue, and a metallic tool model of the da Vinci monopolar curved scissors tool suspended over the tissue. Light sources surrounded the tool shaft, pointing toward the tissue below. Rotations of the tool blocked a percentage of the light that would be incident on the tissue. These simulations were used to determine the influence of tool rotation on fluence and to provide insights into an optimal tool orientation for surgical guidance.

2. METHODS

2.1 Optical Simulations

The Monte Carlo Extreme (MCX) software[26] was employed to simulate a da Vinci scissor tool. This tool was represented by a cylinder and an ellipse, as shown in Fig. 1 which compares our simplified model next to a real da Vinci monopolar curved scissors. The cylinder in our model represents the base of the da Vinci tool tip, and the ellipse represents the segment of the tip where the scissor blades are located. The two joints are referred to as the wrist joint and scissor joint, as shown in Fig. 1 (b). The optical parameters of the tissue were determined using liver tissue parameters determined by Ritz et al.[27]

To determine the impact of orientation angles on fluence, light propagating from the seven fibers (i.e., toward the underlying tissue) was simulated for varying tool orientations. If the tool blocks a light beam path, the light will be absorbed by the tool. When photons reach the underlying tissue, the MCX program produces a value

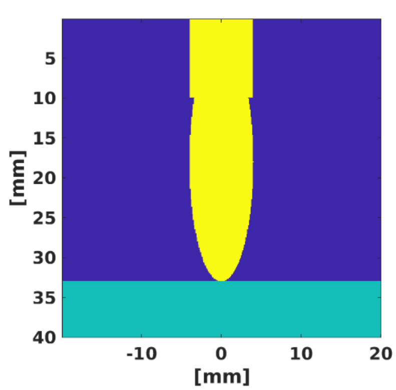

(a)

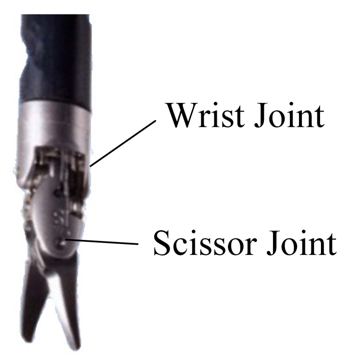

(b)

Figure 1: (a) Cross-sectional image of the simulation environment in MCX. The yellow shapes are the cylinder and ellipse which, collectively, represent the da Vinci bipolar forceps. The blue area represents air and the turquoise represents the biological medium. (b) Image of the da Vinci monopolar curved scissors for comparison.[25]

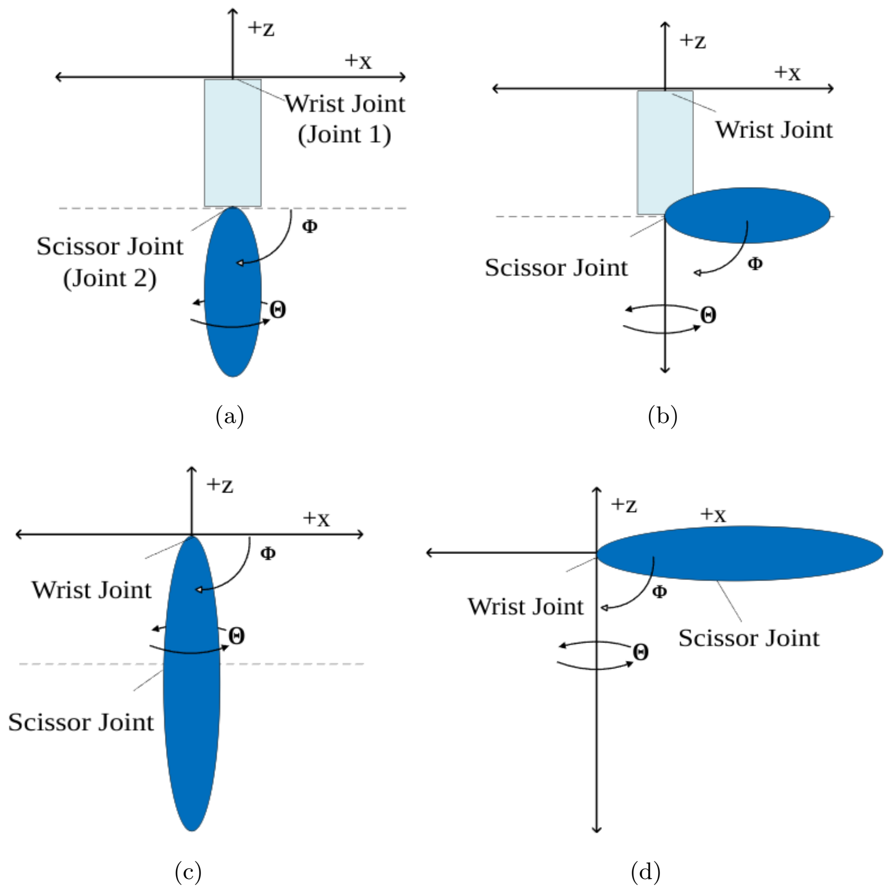

Figure 2: Diagrams of the (a,b) scissor and (c,d) wrist joint rotation models when (a,c) $\Theta = 0°$ and $\Phi = -90°$ and (b,d) $\Theta = 0°$ and $\Phi = 0°$.

of normalized fluence at the tissue boundary based on the initial fluence. Fluence was measured 1 mm below the tissue surface in a region of interest (ROI) defined as a circle of radius 10 mm with the center of the circle aligned with the tool axis.

2.2 Scissor & Wrist Joint Rotations

Without native support for CAD models in MCX, designing a rotating tool presented a challenge. MCX requires mathematical definitions of boundaries between different media and does not support the importation of specific CAD designs. Therefore, to create an object which could change its orientation, a rotational transformation matrix was applied to an ellipse. This allowed the ellipse to rotate with two possible angles, Φ and Θ. The Φ angle refers to rotations around the wrist or scissor joint (i.e., joints 1 or 2, respectively). The Θ angle refers to rotations around the the z-axis. These rotations are illustrated in Fig. 2.

Although joints 1 and 2 were separate when modeling scissor joint rotation, as shown in Figs. 2(a) and 2(b), these two joints were modeled as a single ellipse during wrist joint rotation (i.e., joint 2 was locked at the same Φ angle as joint 1 during Φ or Θ rotations), as shown in Figs. 2(c) and 2(d). These differences were implemented because MCX simulations require cylindrical objects to be defined with the cylindrical axis at angular multiples of 90°. Hence, wrist joint rotations could not accommodate two separate models. However, the scissor joint rotation model includes a cylinder above the scissor joint that can remain fixed at Φ=-90°. As a result of this fixed joint position, the Φ axis of rotation is parallel to the y axis in the scissor joint rotation model.

To simulate different angular orientations, first, Θ was set to 0°, and the tool was rotated through a range of Φ values. Then, Θ was increased to another value and the tool was rotated through the same range of Φ values.

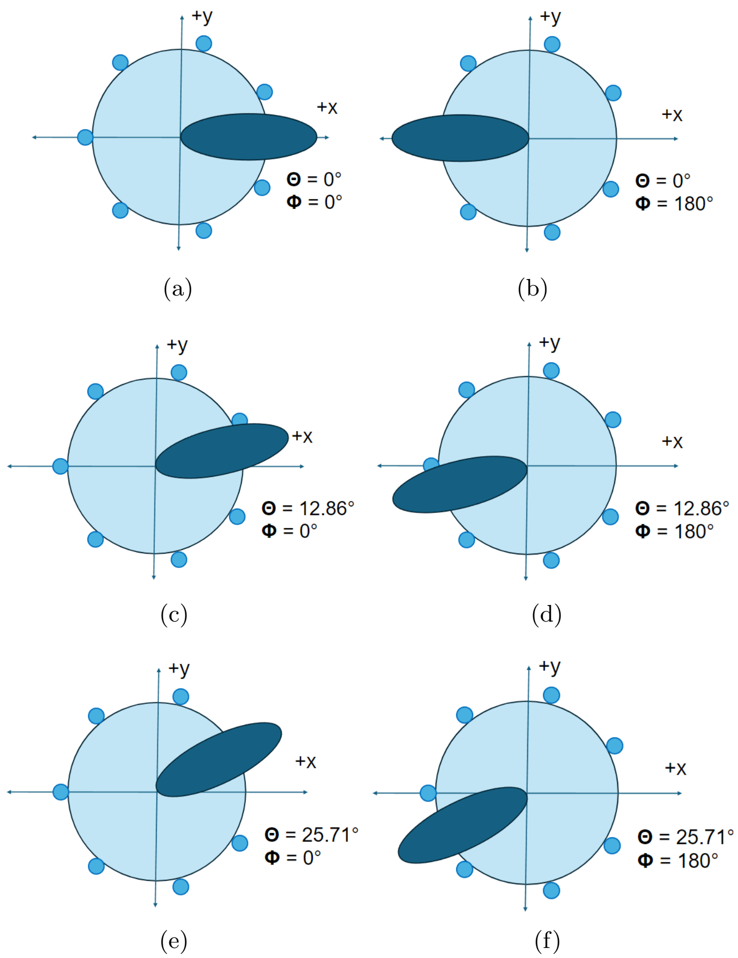

Figure 3: Cross-sectional views of the tool shaft and the seven surrounding optical fiber tips, which are distributed evenly (though not circularly symmetric). Therefore, when the scissor or wrist joint rotates about the y-axis from (a,c,e) Φ=0° to (b,d,f) $\Phi = 180°$, the light profile will be impacted differently based on the Θ value: (a,b) Θ=0°, where the final position of the rotated joint causes tool intersection with the axis of one optical fiber, (c,d) Θ=12.86°, where the rotating joint does not intersect with the axes of any optical fibers, and (e,f) $\Theta = 25.71°$, where the rotating joint initially intersects with the axis of one optical fiber.

This process was repeated for the multiple values of Θ and Φ investigated. As shown in Fig. 3(a), with the tips of seven optical fibers placed to surround the tool wrist and with $\Theta = 0°$, rotating joint 1 or 2 to a value of $\Phi = 0°$ results in the scissor tip residing between two optical fibers. However, as shown in Fig. 3(b), with $\Theta = 0°$, rotating joint 1 or 2 to a value of $\Phi = 180°$, along the path indicated in Fig. 2, causes the scissor tip to reside directly under one optical fiber. Conversely, with $\Theta = 12.86°$, rotating joint 1 or 2 about the y-axis, from $\Phi = 0°$ (Fig. 3(c)) to $\Phi = 180°$ (Fig. 3(d)), does not cause intersection with the axes of any optical fibers. With $\Theta = 25.71°$, rotating joint 1 or 2 about the y-axis, from $\Phi = 0°$ (Fig. 3(e)) to $\Phi = 180°$ (Fig. 3(f)), initially intersects the axis of one optical fiber, then does not intersect with the axes of any optical fibers.

2.3 Simulation Parameters

Of the multiple possible rotations, the Φ rotation is most relevant for fluence transmission to underlying tissue, as joints 1 and 2 can range from $\Phi = -90°$ (i.e., the scissor tool tip blocks minimal light, as shown in Fig. 2(a)) to Φ =0° (Figs. 2(b) and 3(a)) or Φ =180° (Fig. 3(b)). At the angles Φ =0° and Φ =180°, the scissor tool tip could potentially block most of the light transmitted from a single optical fiber, as illustrated in Fig.

3. Conversely, Θ rotation is most relevant to determining whether the tool tip directly blocks one of the seven optical fibers or resides between two optical fiber paths, as illustrated in Fig. 3.

To determine the impact of Θ on fluence, the scissor and wrist joints were rotated from Φ=0° to Φ=-180°, in 18°-degree increments, for multiple possible values of Θ ranging 0° to 25.71°. The Θ range was chosen based on the maximum angular range necessary to achieve unique results, considering the periodicity of the seven fibers surrounding a circular geometry and the Φ range from -180° to 0°, which further limits the number of unique results by a factor of two (i.e., 360°/7/2= 25.71°).

3. RESULTS

Fig. 4(a) shows normalized fluence as a function of the Φ wrist joint rotation angles, for the multiple values of Θ reported in the legend. Normalized fluence within the ROI varied from 0.94 to 1.14, resulting in 18-21% difference among the investigated orientations, relative to the minimum or maximum value. When Φ = -180° or 0°, the fluence values range 0.94 to 1.08, resulting in 8-13% difference among the investigated Θ angles (relative to the maximum or minimum value). As expected, fluence is maximized when Φ = -90° (i.e., when the tip is pointing along the -z axis in Fig. 3), and less light is transmitted as the tool tip rotates away from alignment with the z axis.

When Θ is 0°, 4.29°, or 8.57°, fluence monotonically increases in Fig. 4(a) with Φ values ranging -180° to -144° and -54° to 0° (with each range representing ≥54° excursion from alignment with the z axis). When Θ is 17.14°, 21.43°, and 25.71°, the fluence decreases over the same range of Φ values representing ≥54° excursion from alignment with the z axis. The first set of Θ values are similar to the second set when reflected about Φ = -90° on the abscissa of the plot in Fig. 4(a), while the result obtained with Θ =12.86° is approximately symmetric when reflected about Φ = -90° on the abscissa, representing an optimal Θ value for consistent fluence delivery.

Fig. 4(b) shows normalized fluence as a function of the Φ scissor joint rotation angles. The normalized fluence values range 0.97 to 1.06, resulting in 8-9% difference relative to the minimum or maximum value. Hence, fluence is less impacted by Θ rotations of the scissor joint, relative to Θ rotations of the wrist joint, considering that the scissor joint is farther away from the light source. As expected, fluence monotonically decreases as the scissor joint rotates away from Φ= -90°, as a result of the closer distance between the scissor tool and one or more optical fibers.

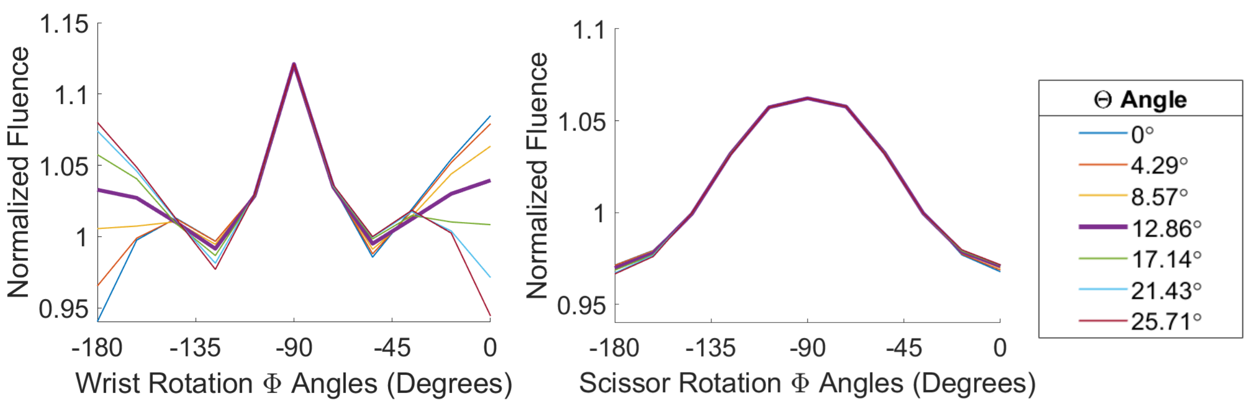

(a) (b)

Figure 4: Normalized fluence measured as a function of (a) wrist and (b) scissor joint rotations, with specific Θ angles shown in the legend. Although both the scissor and wrist joints rotate through same Φ angles, the Φ axis of rotation is located in different places, as shown in Figs. 2(b) and 2(d) (i.e., the Φ axis is located at the scissor joint for tip rotation and at the wrist joint for base rotation).

4. DISCUSSION

This work is the first to investigate the effect of da Vinci tool orientations on fluence when using a tool-attached illumination source. Previous research demonstrates that angular orientation differences can result in >5 dB change in contrast of the corresponding photoacoustic images.[20] Therefore, a robust design for surgical guidance must consider potential changes in fluence to prevent photoacoustic image quality degradation.

The difference between the maximum and minimum normalized fluence values achieved with the simulated tool orientations is approximately 20%. This difference is anticipated to contribute to the discrepancy between photoacoustic images acquired with different tool orientations.[20] Additional contributing factors include the distance between the tool and the target,[20] potential variations in the angles of approach between the tool and target, and the real-time position of a target during surgery.

Although it may be difficult to control tool orientations for a particular surgical procedure, a few optimal options have emerged in cases where multiple orientations are permissible. In particular, during wrist joint rotation (Fig. 4 (a)), Θ=12.86° yields fluence values that are centered between the two limits of periodicity (i.e., Θ=0° and Θ=25.71°). Therefore, to achieve the most consistent fluence delivery as a function of Φ, it is considered optimal to use a Θ value that resides between 0° and 25.71° (e.g., 12.86°).

Limitations of this work include the challenges associated with modeling an angled cylinder, which resulted in geometry that was not completely true to the da Vinci monopolar scissors tool for the wrist joint rotation model. As a result, this model did not allow different Φ angles for the scissor and wrist joints. Therefore, the fluence values reported in Fig. 4(a) represent only one set of values that can be achieved with wrist joint rotations. In addition, based on the results in Fig. 4(b), the two models (i.e., joint and scissor rotation models) produce slightly different results, as the same maximum fluence value would otherwise be achieved with Φ=-90° in both plots (i.e., 1.06 vs. 1.08, which represents a 2% difference).

Future work could potentially quantify the photoacoustic image quality achieved with realistic tool tip orientations, with the goal of validating our findings. Future work may also investigate a range of additional parameters, such as including investigations of the light profiles achieved on the surface of tissue,[28] multiple possible angles between the tool and tissue, and different locations and angles of the optical fibers surrounding the tool with specific tool rotations.

5. CONCLUSION

We successfully demonstrated relative expectations for light blockage when rotating the scissor and wrist joints of a da Vinci scissor tool for photoacoustic-guided surgery. The variation in fluence measured 1 mm below the tissue surface was at most 18-21% with Φ rotations of the wrist joint and 9-13% with Θ rotations of the wrist joint. To achieve consistency in fluence values, 12.86° was determined to be an optimal Θ value when the Φ rotation is ≥54° from alignment with the z-axis. Results enhance our understanding of these critical components of light delivery, which have the potential to impact the associated photoacoustic image quality.

REFERENCES

[1] I. Alkatout, U. Mechler, L. Mettler, *et al.*, "The development of laparoscopy—a historical overview," *Frontiers in surgery* **8**, 799442 (2021).

[2] S. E. Delacroix and J. Winters, "Urinary tract injuries: recognition and management," *Clinics in colon and rectal surgery* **23**(03), 221–221 (2010).

[3] S. Maeso, M. Reza, J. A. Mayol, *et al.*, "Efficacy of the da vinci surgical system in abdominal surgery compared with that of laparoscopy: a systematic review and meta-analysis," *Annals of surgery* **252**(2), 254–262 (2010).

[4] M. A. L. Bell, "Photoacoustic imaging for surgical guidance: principles, applications, and outlook," *Journal of Applied Physics* **128**(6), 060904 (2020).

[5] M. Xu and L. V. Wang, "Photoacoustic imaging in biomedicine," *Review of Scientific Instruments* **77**, 041101 (2006).

[6] R. Bouchard, O. Sahin, and S. Emelianov, "Ultrasound-guided photoacoustic imaging: current state and future development," *IEEE Transactions on Ultrasonics, Ferroelectrics, and Frequency Control* **61**(3), 450–466 (2014).

[7] M. A. L. Bell, A. K. Ostrowski, K. Li, *et al.*, "Localization of transcranial targets for photoacoustic-guided endonasal surgeries," *Photoacoustics* **3**(2), 78–87 (2015).

[8] M. T. Graham, J. Huang, F. X. Creighton, *et al.*, "Simulations and human cadaver head studies to identify optimal acoustic receiver locations for minimally invasive photoacoustic-guided neurosurgery," *Photoacoustics* **19**, 100183 (2020).

[9] B. Eddins and M. A. L. Bell, "Design of a multifiber light delivery system for photoacoustic-guided surgery," *Journal of Biomedical Optics* **22**(4), 041011 (2017).

[10] B. Eddins and M. A. L. Bell, "Optimizing light delivery for a photoacoustic surgical system," in *Photons Plus Ultrasound: Imaging and Sensing*, **10064**, 63–68, SPIE (2017).

[11] K. M. Kempski, A. Wiacek, M. Graham, *et al.*, "In vivo photoacoustic imaging of major blood vessels in the pancreas and liver during surgery," *Journal of Biomedical Optics* **24**(12), 121905 (2019).

[12] K. M. Kempski, A. Wiacek, J. Palmer, *et al.*, "In vivo demonstration of photoacoustic-guided liver surgery," in *Photons Plus Ultrasound: Imaging and Sensing*, **10878**, 205–209, SPIE (2019).

[13] M. A. L. Bell and J. Shubert, "Photoacoustic-based visual servoing of a needle tip," *Scientific Reports* **8**, 15519 (2018).

[14] M. Graham, F. Assis, D. Allman, *et al.*, "In vivo demonstration of photoacoustic image guidance and robotic visual servoing for cardiac catheter-based interventions," *IEEE Transactions on Medical Imaging* **39**(4), 1015–1029 (2020).

[15] M. R. Gubbi, F. Assis, J. Chrispin, *et al.*, "Deep learning in vivo catheter tip locations for photoacoustic-guided cardiac interventions," *Journal of Biomedical Optics* **29**(S1), S11505 (2023).

[16] E. A. González, A. Jain, and M. A. L. Bell, "Combined ultrasound and photoacoustic image guidance of spinal pedicle cannulation demonstrated with intact ex vivo specimens," *IEEE Transactions on Biomedical Engineering* **68**(8), 2479–2489 (2021).

[17] E. González, A. Jain, and M. A. L. Bell, "Photoacoustic differentiation of cortical from cancellous bone in the lumbar vertebrae of an intact human cadaver to prevent bone breaches during spinal fusion surgeries," in *Photons Plus Ultrasound: Imaging and Sensing*, **11642**, 74–80, SPIE (2021).

[18] J. Shubert and M. A. L. Bell, "Photoacoustic imaging of a human vertebra: implications for guiding spinal fusion surgeries," *Physics in Medicine & Biology* **63**(14), 144001 (2018).

[19] A. Wiacek, K. C. Wang, H. Wu, *et al.*, "Photoacoustic-guided laparoscopic and open hysterectomy procedures demonstrated with human cadavers," *IEEE Transactions on Medical Imaging* **40**(12), 3279–3292 (2021).

[20] M. Allard, J. Shubert, and M. A. L. Bell, "Feasibility of photoacoustic-guided teleoperated hysterectomies," *Journal of Medical Imaging* **5**(2), 021213 (2018).

[21] M. Allard, J. Shubert, and M. A. L. Bell, "Feasibility of photoacoustic guided hysterectomies with the da vinci robot," in *Medical Imaging 2018: Image-Guided Procedures, Robotic Interventions, and Modeling*, **10576**, 60–66, SPIE (2018).

[22] A. Wiacek, K. C. Wang, H. Wu, *et al.*, "Parking sensor-inspired approach to photoacoustic-guided hysterectomy demonstrated with human cadavers," in *Photons Plus Ultrasound: Imaging and Sensing*, **11642**, 68–73, SPIE (2021).

[23] N. Gandhi, M. Allard, S. Kim, *et al.*, "Photoacoustic-based approach to surgical guidance performed with and without a da Vinci robot," *Journal of Biomedical Optics* **22**(12), 121606 (2017).

[24] T. Zhao, A. E. Desjardins, S. Ourselin, *et al.*, "Minimally invasive photoacoustic imaging: Current status and future perspectives," *Photoacoustics* **16**, 100146 (2019).

[25] M. T. Wooju Jeong and C. G. Rogers, "Robotic surgery: Basic instrumentation and troubleshooting," (2023).

[26] Q. Fang and D. A. Boas, "Monte carlo simulation of photon migration in 3d turbid media accelerated by graphics processing units," *Opt. Express* **17**, 20178–20190 (2009).

[27] J.-P. Ritz, A. Roggan, C. Isbert, *et al.*, "Optical properties of native and coagulated porcine liver tissue between 400 and 2400 nm," *Lasers in Surgery and Medicine: The Official Journal of the American Society for Laser Medicine and Surgery* **29**(3), 205–212 (2001).

[28] G. C. Keene and M. A. L. Bell, "Optimizing light delivery to perform teleoperative photoacoustic-guided hysterectomy," in *Proceedings of SPIE Photonics West*, SPIE (2025).